Deep phenotyping in zebrafish reveals genetic and diet-induced adiposity changes that may inform disease risk

Deep phenotyping in zebrafish reveals genetic and diet-induced adiposity changes that may inform disease risk

James E. N. Minchin[1,2*], Catherine M. Scahill[3], Nicole Staudt[3], Elisabeth M. Busch-Nentwich[3,4] & John F. Rawls[2]

[1]Centre for Cardiovascular Science, University of Edinburgh, Edinburgh, UK, EH16 4TJ, [2]Department of Molecular Genetics and Microbiology, Duke University, Durham, NC, USA, 27710, [3]Wellcome trust Sanger Institute, Wellcome Genome Campus, Hinxton, UK, CB10 1SA, [4]Department of Medicine, University of Cambridge, Cambridge, UK, CB2 0QQ

*Author for correspondence: james.minchin@ed.ac.uk

Abstract

The regional distribution of adipose tissues is implicated in a wide range of diseases. For example, proportional increases in visceral adipose tissue increase the risk for insulin resistance, diabetes and cardiovascular disease. Zebrafish offer a tractable model system by which to obtain unbiased and quantitative phenotypic information on regional adiposity, and deep phenotyping can explore complex disease-related adiposity traits. To facilitate deep phenotyping of zebrafish adiposity traits, we used pairwise correlations between 67 adiposity traits to generate stage-specific adiposity profiles that describe changing adiposity patterns and relationships during growth. Linear discriminant analysis classified individual fish according to adiposity profile with 87.5% accuracy. Deep phenotyping of eight previously uncharacterized zebrafish mutants identified *neuropilin 2b* as a novel gene that alters adipose distribution. When we applied deep phenotyping to identify changes in adiposity during diet manipulations, zebrafish that underwent food restriction and re-feeding had widespread adiposity changes when compared to continuously-fed, equivalently-sized control animals. In particular, internal adipose tissues (e.g., visceral adipose) exhibited a reduced capacity to replenish lipid following food restriction. Together, these results in zebrafish establish a new deep phenotyping technique as an unbiased and quantitative method to help uncover new relationships between genotype, diet and adiposity.

Introduction

Adipose tissues (ATs) are lipid-rich organs that supply and sequester circulating lipid in response to systemic energy demands. ATs thus provide 'energetic insurance' to individuals, and confer selective advantages during periods of adverse physiological stresses. In modern societies, where food availability is high and energy expenditure is low, ATs accumulate large quantities of lipid which can initiate a range of secondary metabolic abnormalities that result in increased susceptibility to diabetes, cardiovascular disease (CVD) and cancer. A wide-range of adiposity traits can influence disease risk. For example, general adiposity levels, as measured by body mass index (BMI), are associated with increased risk for disease (1). In turn, the regional distribution of AT can also influence disease risk. For example, accumulation of visceral adipose tissue (VAT) in the abdominal cavity in close proximity to visceral organs, is associated with an increased risk for insulin resistance and a sequelae of accompanying diseases such as diabetes and CVD (2, 3). Conversely, accumulation of subcutaneous adipose tissue (SAT) in a peripheral location at the hips and upper thighs, is associated with reduced disease risk (4). Understanding how genetics and the environment influence these diverse adiposity traits will be key to treating and predicting the metabolic consequences of obesity.

Zebrafish are a tropical freshwater fish that offer a tractable model system to study AT biology. Zebrafish AT is morphologically and molecularly homologous to mammalian white adipose tissue (5, 6). Zebrafish AT also appears to be functionally conserved to mammalian WAT and accumulates lipid during periods of chronic energy excess, and mobilizes lipid during energy deficiency (5, 7, 8). The molecular pathways that regulate

adiposity also appear to be conserved between zebrafish and mammals, as typified by zebrafish *growth hormone* (*gh*) mutants (9). Importantly, zebrafish AT can be visualized and quantified in vivo at both cell and whole-animal resolutions (10, 11). We recently utilized these imaging properties to comprehensively identify, characterize and quantify the full complement of zebrafish ATs at distinct developmental stages (7). This methodology generates unbiased and quantitative phenotypic information on a comprehensive range of adiposity traits. We reasoned that such multivariate data could be utilized for deep phenotyping of adiposity traits. Briefly, deep phenotyping is defined as the precise and comprehensive analysis of phenotypic abnormalities (12), and is useful for identifying traits and complex phenotypic signatures that define health or disease (13-15). Deep phenotyping is particularly powerful when such traits may be quantitative and subtle, as found with adiposity.

In this study, we generated stage-specific adiposity profiles that comprehensively capture patterns and relationships in adiposity dynamics and adipose distribution. To classify individuals according to expected patterns of adiposity, we applied linear discriminant analysis (LDA) to the adiposity profiles. We utilized this methodology to screen eight zebrafish mutants, and identified *neuropilin 2b* (*nrp2b*) as a novel gene that promotes adiposity in zebrafish. Finally, we applied our deep phenotyping strategy to identify adiposity changes that occur following diet manipulation. We identified that food restriction induced profound changes in fat distribution even after animals had fully re-gained weight. Closer analysis revealed that Internal ATs (IATs), including VAT, did not fully re-gain lipid following re-feeding resulting in altered fat distribution. Altogether, we

develop methodology to quantitatively extract phenotypic information for detecting gene and diet-induced adiposity phenotypes.

Materials & Methods

Zebrafish husbandry, strains and data availability

Zebrafish experiments conformed to the U.S. Public Health Service Policy on the Humane Care and Use of Laboratory Animals, using protocols approved by the Institutional Animal Care and Use Committees of the University of North Carolina at Chapel Hill (UNC) and Duke University. Zebrafish husbandry for experiments conducted at either UNC or Duke were performed as previously described (7). The Ekkwill (EKW) and WIK wild-type data used as the LDA training set (*N* = 456) was previously published (7), and is available for download at DataDryad (DOI: https://doi.org/10.5061/dryad.98470). The *gh* mutant data used as a positive control for LDA were previously published (9) and raw images are available for download at DataDryad (***not yet deposited***). The eight zebrafish mutants used for LDA were obtained from the Wellcome Trust Sanger Institute's Zebrafish Mutation Project (ZMP) or from ZIRC (16). Embryos were received at Duke on a Hubrecht long-fin background (HLF). Incrosses were performed between heterozygous individuals to generate experimental clutches. Genotypes were determined by Sanger sequencing. Images used for quantification are deposited at DataDryad (***not yet deposited***). All alleles used in this study are included in **Table 1**. The food restriction and re-feeding was performed in EKW wild-type fish at Duke and the raw images are available for download at DataDryad (***not yet deposited***).

Nile Red staining, image analysis, adipose and stage classification

Nile Red (Sigma-Aldrich, #N1142) was dissolved in acetone at 1.25 mg/ml and diluted to 0.5 µg/ml in system water for lipid staining (10, 11). Zebrafish were incubated in the diluted Nile Red for 30 minutes as previously described (10, 11). Following the staining, melanosomes were contracted by incubation in 10 mg/ml epinephrine (Sigma-Aldrich, #E4375) for 5 minutes, and zebrafish were anaesthetized in 1.34 g/L MS222 (Sigma-Aldrich, #A5040) for 3 minutes and mounted on 3% methylcellulose (Sigma-Aldrich, #MO387). The right-hand side of each fish was imaged on a Leica MZ205FA fluorescence stereomicroscope equipped with a Leica DFC365 FX fluorescence camera, and using a GFP2 bandpass filter (Leica Microsystems, #10447407). All analyses were conducted in FIJI/ImageJ (v1.51i) (17). For AT area measurements, two copies of each image were opened; one for taking measurements, and one for comparisons to maximize accuracy of adipose segmentation. Standard length (SL), height at the anterior margin of the anal fin (HAA), and body area were used to determine zebrafish size and were measured using the line and polygon tools as previously described (7, 18). AT areas were defined by manually set thresholds based on pixel intensities (7). For ATs that did not touch, the magic wand tool was used to select AT area. For touching ATs, the polygon tool was used to trace the AT outline, and where a dividing line between the ATs was not visible, a straight line was drawn between the farthest distinguishing AT points. Lateral view images were used for all measurements. ATs were classified and measured as described here (7). A schematic illustrating the location of each AT in zebrafish is included in **Supplemental Figure 1**. The stages used for generating adiposity profiles incorporated both postembryonic and adiposity milestones as previously documented (7, 18). As previously described, Nile Red also labels neutral lipid within the liver, intestinal

epithelium and the blood (5, 7); however, lipid at these sites can be readily distinguished from AT. Adiposity measurements used in this study are included in **Supplemental Tables 1 and 2**.

Food restriction and re-feeding experiments

Food restriction and re-feeding experiments were conducted largely as described (5), with the following differences; zebrafish at 38 days post fertilization (11.4 ± 0.5 mm SL (mean ± standard deviation); DFRSAT stage) were housed individually in six-well plates containing ~3 ml of system water. No food was administered during food restriction (days 1–11). Upon re-feeding (days 12–22), fish were fed *Artemia franciscana* and powdered food as per normal husbandry procedures at Duke University as previously described (7). Every 24 hours, 0.5 µg/ml Nile Red was added to the wells, and the fluorescent lipid signal was imaged on a Leica MZ205FA fluorescence stereomicroscope equipped with a Leica DFC365 FX fluorescence camera as described above. Lipid deposits were thus evaluated daily and food restriction was stopped after 11 days once lipid was mobilized from all AT sites in all animals. System water was replaced daily during both starvation and re-feeding periods.

Statistical analyses

Stage-specific adiposity profiles were generated using pairwise correlations between 63 adiposity traits (listed in **Table 2**) using the multivariate platform in JMP Pro 13 (SAS, NC). Adiposity profiles were constructed for 14 stages (**Supplemental Figure**

2 and Supplemental Tables 3-16). Heatmaps to visualize the adiposity profiles were generated in JMP and show pairwise inter-trait correlations expressed as the Pearson's correlation coefficient (1 is a total positive correlation between traits, 0 is no correlation, -1 is a total inverse correlation). LDA was performed to classify individual fish according to their adiposity profiles. LDA was performed in JMP using the discriminant analysis platform and a linear common covariance method. LDA is a general linear model that derives discriminant functions - linear combinations of variables - to maximize the probability of assigning observations to a pre-defined group. The discriminant functions for each group (adiposity profile) ($C_{profile}$) followed (19, 20), and are expressed as: $C_{profile} = i + c_1(\log_{10} a_1) + c_2(\log_{10} a_2) + \cdots + c_n(\log_{10} a_n)$ where c is the coefficient of the classification equation (19), i is the constant for each group (adiposity profile) as determined by multiplying the matrix of classification coefficients for that group by the matrix of means for each adiposity trait variable (a) of that group. All 63 adiposity traits were used as variables for LDA. To define the adiposity characteristics, adiposity profiles from 456 wild-type fish were set as a validation group (training set). Analysis of inter-clutch variability in LDA within the training set revealed misclassification rates of 15.2% (mean) with a standard error (SE) of 2.4% (25 independent clutches). This baseline rate was used to identify phenotypic fish during additional comparisons. We defined 'non-normal' phenotypes if clutches had a % misclassification rate >3 ± SE from the training set rate. These clutches were evaluated further as phenotypic. Principal components analysis (PCA) of adiposity profiles during food restriction (days 1-11) and re-feeding (days 12-22) was conducted in JMP using the default estimation method. The mean recovery, or re-gain, of AT-lipid at day 22 (following food restriction and re-feeding) was

calculated as a % of AT-lipid at day 1. Hierarchical clustering of AT-lipid re-gain at day 22 was performed in JMP using the Ward method (21). Student's t-tests were used for pairwise comparisons, and one-way ANOVA followed by Tukey's post-hoc test used for multiple groups. ANCOVA was used to test for differences between groups following linear regression. Statistical significance was set to alpha = 0.05. Graphs were plotted in R using ggplot2 (22, 23). The stage-specific adiposity profiles can be found in **Supplemental Figure 2** and the accompanying correlation matrices in **Supplemental Tables 3-18**

Results

Stage-specific phenotypic profiles capture adiposity patterns and relationships

Whole-animal in vivo imaging in zebrafish enables the quantification of all ATs in a single animal and can thus be used to reveal a wide range of adiposity traits, including changes in fat levels, ectopic localization to specific organs and changes in regional distribution (5, 10, 11). We reasoned that collecting large amounts of quantitative adiposity data could be used to classify individuals based on adiposity traits and identify subtle, quantitative adiposity phenotypes. We previously showed that stage-matched zebrafish exhibit stereotypical adiposity patterns (**Fig. 1A**) (7). Therefore, we utilized existing data to generate stage-specific phenotypic profiles that capture adiposity information (hereafter called adiposity profiles). In total, 456 wild-type zebrafish across a range of sizes, stages and ages were used to construct adiposity profiles (**Fig. 1B**) (7). From these 456 fish, 67 traits were quantified in each fish (**Table 1**). The 67 traits included (i) AT area measurements, (ii) measures of body size (including SL, HAA, body area), (iii) composite AT groupings (e.g., total AT, SAT, VAT), and (iv) AT proportionality assessments (e.g., VAT:SAT). Correlations were computed between each trait and assessed to determine how adiposity relationships and patterns change in fish of distinct stages (**Fig. 1B**). As expected, considerable differences were observed in adiposity profiles at distinct stages (**Fig. 1B & C**). For example, Pancreatic VAT (PVAT) was initially positively correlated with SL (stage PB), before becoming progressively more inversely correlated with SL in larger fish (stage SA) (**Fig. 1C**). In conclusion, adiposity profiles capture dynamic changes in adiposity patterns at distinct developmental stages and will be useful indicators of ‘normal’ adiposity levels and variation.

Linear discriminant analysis accurately classifies zebrafish according to the adiposity profile

To effectively use stage-specific adiposity profiles as a base for in-depth phenotypic profiling we utilized linear discriminant analysis (LDA). LDA is a data dimensionality reduction technique that can assign membership of a group based on accompanying covariate values. LDA has been used previously to (i) classify morphological phenotypes into distinct groups (24, 25), (ii) predict disease outcomes based on current symptoms (26), and (iii) predict future business success based on current financial parameters (27). We reasoned that LDA could also be applied to adiposity profiles and used to classify individual fish according to expected adiposity traits. As a training set, we applied the adiposity profiles from the 456 wild-type fish described above and assessed whether LDA was able to accurately assign fish to correct developmental stages (**Fig. 2A**). Based on adiposity profiles, LDA assigned 87.5% of the wild-type fish into correct stages (**Fig. 2A**). We next assessed how robust the LDA classification method was across multiple independent clutches. We divided the training set data into its 25 constituent clutches and applied LDA to each clutch, resulting in an average classification rate of 84.8 ± 2.4% (mean ± SE) (**Fig. 2E**). Next, as a proof-of-concept, we used zebrafish *growth hormone* (*gh*) mutants to determine if LDA can be used to detect adiposity phenotypes. We previously showed that *gh* mutants have increased adiposity and retarded somatic growth relative to size-matched wild-type siblings (**Fig. 2B & C**) (9). From McMenamin et al. we applied LDA to the adiposity profiles of 62 homozygous *gh* mutants and 60 wild-type siblings from three clutches (**Fig. 2D**).

Adiposity profiles from the 456 wild-type zebrafish were used as a training set (**Fig. 2D**). Within the training set, LDA identified 15.2% of animals as phenotypic, setting a low background misclassification rate (**Fig. 2E**). From the *gh* mutant-only data, LDA correctly identified phenotypes based on adiposity profiles in 60% of cases (**Fig. 2E**). However, when the clutch was considered as a whole (containing both wild-type siblings and mutants), LDA classified 36% of individuals as phenotypic (P = 0.003) (**Fig. 2E**). Based on the genotype data, the true misclassification rate was expected to be 50.8%; therefore, although LDA was underperforming, it could be effectively used to flag the clutch as phenotypic. Taken together, LDA can be used to identify phenotypic adiposity traits based on adiposity profiles.

Identification of *nrp2b* as a novel gene implicated in zebrafish adiposity

We next sought to apply LDA to help identify novel zebrafish adipose mutants. We obtained eight mutant lines generated by the Zebrafish Mutation Project (ZMP) (**Table 1**) (16). The eight ZMP mutants were selected as candidate regulators of adiposity based on published experimental evidence or by genome-wide association studies (28-35). Heterozygous carriers from the ZMP mutants were intercrossed, the offspring raised to ~30 days post fertilization (dpf) and then Nile Red was used to visualize AT levels (**Fig. 3**). Following imaging, the fish were genotyped to identify wild-type, heterozygous and homozygous mutants. Adiposity profiles were constructed for each fish, and LDA used to identify differences in adiposity relative to the training set of 465 wild-type fish. Of the eight ZMP mutant lines, only *nrp2b* robustly presented mutant identification rates higher than expected from wild-type fish (**Fig. 3A**), suggesting that mutation of *nrp2b* may

influence adiposity in zebrafish. The other seven lines all exhibited misclassification rates within the expected wild-type range and were therefore classed as phenotypically normal (**Fig. 3A**). Closer analysis of the *nrp2b* fish stained by Nile Red revealed a robust reduction in total adiposity, which was validated by analyzing two additional and independent clutches (**Fig. 3B & C**). In conclusion, we utilized LDA to screen eight new zebrafish mutants for adiposity phenotypes and identified *nrp2b* as a potential novel modifier of adiposity.

Linear discriminant analysis identifies differences in adiposity traits following food restriction and re-feeding

We reasoned that adiposity profiles and analysis by LDA could also be applied to identify diet-induced changes in adiposity. To test this, we subjected zebrafish to prolonged food restriction followed by re-feeding until total adiposity levels were completely replenished. Previous studies have shown that zebrafish robustly mobilize and re-gain AT-localized lipid in response to food levels (5). Further, zebrafish recover from acute food restriction with no visible health detriments (5). We subjected 10 wild-type (EKW) zebrafish to complete food restriction for 11 days, followed by 11 days of re-feeding (**Fig. 4**). To build an accurate depiction of adiposity dynamics, the fish were stained with Nile Red and their AT-localized lipid imaged daily during the course of the diet manipulation (**Fig. 4A**). AT-localized lipid was fully mobilized by 11 days of food restriction, as judged by the lack of Nile Red+ lipid within adipose tissue (**Fig. 4A**). At this point, zebrafish were re-fed a normal diet (see Methods) until total adiposity had reached levels equivalent to size-matched normally-fed individuals (**Figs. 4A and 5A**). Adiposity profiles were generated

for each fish at each day of diet manipulation (day 1 – 22), and principal components analysis (PCA) was used to identify whether adiposity trait dynamics were different during food restriction and re-feeding (**Fig. 4B & C**). Strikingly, PCA traced distinct trajectories for food restricted and re-fed zebrafish which did not overlap (**Fig. 4B & C**), suggesting that food restriction and re-feeding elicits changes in AT distribution even after complete recovery of total AT levels. We next applied LDA to determine if adiposity profiles differed after food restriction and re-feeding. We generated adiposity profiles of fully re-fed animals (day 22) and 'continuously fed' animals that were matched for both size (SL) and developmental stage (**Fig. 5B and Supplemental Tables 17 & 18**). LDA misclassified ~90% of food restricted and re-fed zebrafish (day 22) when compared with stage-matched control animals (**Fig. 5C**). Thus food restriction and re-feeding leads to wide-ranging adiposity differences relative to normally fed animals.

Differential capacities to replenish lipid post-food restriction lead to fat distribution differences in zebrafish

As food restriction and re-feeding alters fat distribution even after total adiposity levels have been restored, we next closely assessed how individual ATs responded to diet manipulation. We previously identified 34 regionally distinct zebrafish ATs that could be classified into two main divisions; 'internal' (IAT), which contains the VAT, and SAT (7). Calculation of the % recovery of each AT (day 22 levels relative to day 1 levels) revealed that IATs had a more limited capacity to replenish lipid when compared to SAT (**Fig. 6A**). The exception to this was cardiac VAT (CVAT) which exhibited very high levels of lipid replenishment following re-feeding (**Fig. 6A**). When food restricted and re-fed

animals (day 22) were compared to size-matched ‘continuously-fed’ animals it become clear that IAT was unable to recover lipid levels to wild-type levels (**Fig. 6B**), whereas, SAT exhibited robust levels of replenishment to wild-type levels (**Fig. 6C**). Indeed, the average IAT recovery was ~80%, whereas SAT recovery was ~160% (**Fig. 6D**). These distinct capacities to replenish lipid following food restriction and re-feeding resulted in a reduced IAT:SAT ratio when compared to stage-matched ‘continuously-fed’ control fish (**Fig. 6E**). Taken together, food restriction and re-feeding led to altered fat distribution even after full replenishment of AT levels. These changes were caused by a general failure of internal ATs to replenish lipid levels.

Discussion

Deep phenotyping offers considerable potential for the identification of parameters that signify health and disease. Comprehensive and quantitative phenotyping methods are particularly important for adiposity traits that often exhibit complex and continuous phenotypes that are often not adequately assessed by qualitative methods. In this study, we utilize in vivo imaging in zebrafish to develop adiposity profiles that capture unique patterns and relationships that define an individual's adiposity. We further employ LDA to assign individuals based on adiposity phenotype, and develop this methodology to screen for both genetic and diet-induced changes in adiposity.

Developing quantitative methodology that can robustly evaluate complex morphological and functional phenotypic changes is essential for understanding and interpreting health and disease states. Most studies have so far focused on 'large-effect' phenotypes. However, for complex quantitative traits, phenotypes are often subtler (15). Adiposity is a continuous, complex, quantitative trait; therefore, suitable phenotyping methods are needed. The methodology reported here leverages our recent identification and developmental analysis of zebrafish ATs to generate integrated adiposity profiles for individuals (7). The adiposity profiles generated in this study, capture the patterns and relationships that define an individual's adiposity, and can thus be used to define expected adiposity. LDA represents a tractable strategy to assign individuals to groups according to adiposity profile. Indeed, we found that LDA robustly and accurately classified individuals with a low basal misclassification rate of 12.5%. *gh* mutants were used as a positive control and LDA was able to classify. Therefore, LDA appears to be a robust method to identify multiple aspects of a pleiotropic phenotype. To maximize the

deep phenotyping methods described here it will be helpful to develop automated image analysis methods. Automating accurate segmentation of zebrafish ATs is challenging, owing to their irregular shape; however, the large signal to noise ratio of fluorescent lipophilic dyes, such as Nile Red, are ideal reagents to facilitate automated image segmentation.

As a proof-of-principle, we evaluated whether adiposity profiles and LDA were useful as phenotyping methods in a genetic screen. In total, we tested eight ZMP mutants which have not been previously implicated in adiposity changes. LDA was able to identify a single mutant in *nrp2b* as having an adiposity phenotype. Closer analysis revealed that *nrp2b* has fairly subtle defects in total AT and VAT which were difficult to detect by eye. Neuropilins (Nrps) are co-receptors for secreted Semaphorin ligands, and co-bind with Plexin receptors. Nrps have been implicated in neurogenesis and angiogenesis (36, 37); however, no role has so far been found in adiposity. We recently identified that Plexin D1 (*plxnd1*) mutant zebrafish have altered regional adiposity, characterized by reduced levels of VAT (38, 39). We speculate that Nrp2b in zebrafish may be involved in Plxnd1-mediated VAT growth, possibly by facilitating that binding of Sema3 ligands to the Plxnd1 receptor. Importantly, we did not verify the effect of mutation on the affected gene. This was due to keeping the screen higher-throughput, but leads to the caveat that the specific alleles tested may not lead to large effects (i.e., loss of transcript or protein) (40). Therefore, our results should be interpreted that the tested alleles have no phenotypes, but do not necessarily represent the function of the gene. Evaluating adiposity phenotypes with additional alleles will be essential for properly determining gene function.

As an additional proof-of-principle, we used LDA to assess the effects of food restriction and re-feeding to induce widespread adiposity changes. Food restriction and re-feeding in mammalian models can lead to AT distribution differences (41, 42). For example, calorie restriction or alternate-day fasting in mouse results in preferential visceral fat loss (43). In zebrafish, we identified a striking phenotype whereby internal ATs, which are mainly composed of VAT, do not fully replenish lipid following re-feeding. These changes were evident even in animals with equivalent total levels of AT as normally fed individuals. SATs have a greater capacity to re-deposit lipid when compared to VATs, and re-fed fish display decreased IAT:SAT ratios. As accumulation of SAT is associated with reduced risk of metabolic disease in humans (4) and zebrafish (38), our results raise the possibility that the increased SAT accumulation induced by long-term food restriction and refeeding may have beneficial health effects.

In conclusion, we present here a new method to comprehensively assess the adiposity phenotype in zebrafish. This methodology takes advantage of the fact that a wide range of adiposity traits can be quickly and accurately quantified in live zebrafish, thus providing a complete read-out of an individual's adiposity profile. We anticipate that this method will be useful to identify additional new genetic and environmental factors governing AT development and physiology.

Acknowledgements

We thank the Zebrafish International Resource Center for providing mutant alleles and Steven Farber at the Carnegie Institution for helpful discussions. This work was supported by a British Heart Foundation/University of Edinburgh Fellowship to JENM, a Diabetes UK Early Career Small Grant to JENM (16/0005494), American Heart Association postdoctoral fellowships to JENM (11POST7360004 and 13POST16930097), a Wellcome Trust grant to EBN (206194), and grants from the National Institutes of Health grants (R01-DK093399 to EBN and JFR; R56-DK091356 and R21-ES023369 to JFR).

References

1. Gadde, K. M., C. K. Martin, H. R. Berthoud, and S. B. Heymsfield. 2018. Obesity: Pathophysiology and Management. *J Am Coll Cardiol* **71**: 69-84.

2. Fox, C. S., J. M. Massaro, U. Hoffmann, K. M. Pou, P. Maurovich-Horvat, C. Y. Liu, R. S. Vasan, J. M. Murabito, J. B. Meigs, L. A. Cupples, R. B. D'Agostino, Sr., and C. J. O'Donnell. 2007. Abdominal visceral and subcutaneous adipose tissue compartments: association with metabolic risk factors in the Framingham Heart Study. *Circulation* **116**: 39-48.

3. Karpe, F., and K. E. Pinnick. 2015. Biology of upper-body and lower-body adipose tissue--link to whole-body phenotypes. *Nat Rev Endocrinol* **11**: 90-100.

4. McLaughlin, T., C. Lamendola, A. Liu, and F. Abbasi. 2011. Preferential fat deposition in subcutaneous versus visceral depots is associated with insulin sensitivity. *J Clin Endocrinol Metab* **96**: E1756-1760.

5. Flynn, E. J., 3rd, C. M. Trent, and J. F. Rawls. 2009. Ontogeny and nutritional control of adipogenesis in zebrafish (Danio rerio). *J Lipid Res* **50**: 1641-1652.

6. Imrie, D., and K. C. Sadler. 2010. White adipose tissue development in zebrafish is regulated by both developmental time and fish size. *Dev Dyn* **239**: 3013-3023.

7. Minchin, J. E., and J. F. Rawls. 2017. A classification system for zebrafish adipose tissues. *Dis Model Mech*.

8. Oka, T., Y. Nishimura, L. Zang, M. Hirano, Y. Shimada, Z. Wang, N. Umemoto, J. Kuroyanagi, N. Nishimura, and T. Tanaka. 2010. Diet-induced obesity in zebrafish shares common pathophysiological pathways with mammalian obesity. *BMC Physiol* **10**: 21.

9. McMenamin, S. K., J. E. Minchin, T. N. Gordon, J. F. Rawls, and D. M. Parichy. 2013. Dwarfism and increased adiposity in the gh1 mutant zebrafish vizzini. *Endocrinology* **154**: 1476-1487.

10. Minchin, J. E., and J. F. Rawls. 2011. In vivo analysis of white adipose tissue in zebrafish. *Methods Cell Biol* **105**: 63-86.

11. Minchin, J. E., and J. F. Rawls. 2017. In vivo imaging and quantification of regional adiposity in zebrafish. *Methods Cell Biol* **138**: 3–27.

12. Robinson, P. N. 2012. Deep phenotyping for precision medicine. *Hum Mutat* **33**: 777-780.

13. Hur, M., C. A. Gistelinck, P. Huber, J. Lee, M. H. Thompson, A. T. Monstad-Rios, C. J. Watson, S. K. McMenamin, A. Willaert, D. M. Parichy, P. Coucke, and R. Y. Kwon. 2018. MicroCT-Based Phenomics in the Zebrafish Skeleton Reveals Virtues of Deep Phenotyping in a Distributed Organ System. *Zebrafish* **15**: 77-78.

14. Hur, M., C. A. Gistelinck, P. Huber, J. Lee, M. H. Thompson, A. T. Monstad-Rios, C. J. Watson, S. K. McMenamin, A. Willaert, D. M. Parichy, P. Coucke, and R. Y. Kwon. 2017. MicroCT-based phenomics in the zebrafish skeleton reveals virtues of deep phenotyping in a distributed organ system. *Elife* **6**.

15. San-Miguel, A., P. T. Kurshan, M. M. Crane, Y. Zhao, P. T. McGrath, K. Shen, and H. Lu. 2016. Deep phenotyping unveils hidden traits and genetic relations in subtle mutants. *Nat Commun* **7**: 12990.

16. Kettleborough, R. N., E. M. Busch-Nentwich, S. A. Harvey, C. M. Dooley, E. de Bruijn, F. van Eeden, I. Sealy, R. J. White, C. Herd, I. J. Nijman, F. Fenyes, S. Mehroke, C. Scahill, R. Gibbons, N. Wali, S. Carruthers, A. Hall, J. Yen, E. Cuppen, and D. L.

Stemple. 2013. A systematic genome-wide analysis of zebrafish protein-coding gene function. *Nature* **496**: 494-497.

17. Schindelin, J., I. Arganda-Carreras, E. Frise, V. Kaynig, M. Longair, T. Pietzsch, S. Preibisch, C. Rueden, S. Saalfeld, B. Schmid, J. Y. Tinevez, D. J. White, V. Hartenstein, K. Eliceiri, P. Tomancak, and A. Cardona. 2012. Fiji: an open-source platform for biological-image analysis. *Nat Methods* **9**: 676-682.

18. Parichy, D. M., M. R. Elizondo, M. G. Mills, T. N. Gordon, and R. E. Engeszer. 2009. Normal table of postembryonic zebrafish development: staging by externally visible anatomy of the living fish. *Dev Dyn* **238**: 2975-3015.

19. Tabachnick, B., and L. Fidell. 1996. Using Multivariate Statistics. 3rd Edition ed. Harper & Row, New York.

20. Quinn, G. P., and M. J. Keough. 2002. Experimental Design and Data Analysis for Biologists Cambridge University Press.

21. Murtagh, F., and P. Legendre. 2014. Ward's Hierarchical Agglomerative Clustering Method: Which Algorithms Implement Ward's Criterion? *Journal of Classification* **31**: 274-295.

22. Wickham, H. 2009. ggplot2: Elegant Graphics for Data Analysis Springer-Verlag New York.

23. R Core Team. 2013. R: A language and environment for statistical computing. R Foundation for Statistical Computing. *In*.

24. Bertsatos, A., C. Papageorgopoulou, E. Valakos, and M. E. Chovalopoulou. 2018. Investigating the sex-related geometric variation of the human cranium. *Int J Legal Med*.

25. Suhail, Z., E. R. E. Denton, and R. Zwiggelaar. 2018. Classification of micro-calcification in mammograms using scalable linear Fisher discriminant analysis. *Med Biol Eng Comput*.

26. Oh, J., D. Cho, J. Park, S. H. Na, J. Kim, J. Heo, C. S. Shin, J. J. Kim, J. Y. Park, and B. Lee. 2018. Prediction and early detection of delirium in the intensive care unit by using heart rate variability and machine learning. *Physiol Meas*.

27. Kočišová, K., and M. Mišanková. 2014. Discriminant analysis as a tool for forecasting companys financial health *Procedia - Social and Behavioral Sciences* **110**: 1148-1157.

28. Shungin, D., T. W. Winkler, D. C. Croteau-Chonka, T. Ferreira, A. E. Locke, R. Magi, R. J. Strawbridge, T. H. Pers, K. Fischer, A. E. Justice, T. Workalemahu, J. M. Wu, M. L. Buchkovich, N. L. Heard-Costa, T. S. Roman, A. W. Drong, C. Song, S. Gustafsson, F. R. Day, T. Esko, T. Fall, Z. Kutalik, J. Luan, J. C. Randall, A. Scherag, S. Vedantam, A. R. Wood, J. Chen, R. Fehrmann, J. Karjalainen, B. Kahali, C. T. Liu, E. M. Schmidt, D. Absher, N. Amin, D. Anderson, M. Beekman, J. L. Bragg-Gresham, S. Buyske, A. Demirkan, G. B. Ehret, M. F. Feitosa, A. Goel, A. U. Jackson, T. Johnson, M. E. Kleber, K. Kristiansson, M. Mangino, I. Mateo Leach, C. Medina-Gomez, C. D. Palmer, D. Pasko, S. Pechlivanis, M. J. Peters, I. Prokopenko, A. Stancakova, Y. Ju Sung, T. Tanaka, A. Teumer, J. V. Van Vliet-Ostaptchouk, L. Yengo, W. Zhang, E. Albrecht, J. Arnlov, G. M. Arscott, S. Bandinelli, A. Barrett, C. Bellis, A. J. Bennett, C. Berne, M. Bluher, S. Bohringer, F. Bonnet, Y. Bottcher, M. Bruinenberg, D. B. Carba, I. H. Caspersen, R. Clarke, E. W. Daw, J. Deelen, E. Deelman, G. Delgado, A. S. Doney, N. Eklund, M. R. Erdos, K. Estrada, E. Eury, N. Friedrich, M. E. Garcia, V. Giedraitis, B. Gigante, A. S. Go,

A. Golay, H. Grallert, T. B. Grammer, J. Grassler, J. Grewal, C. J. Groves, T. Haller, G. Hallmans, C. A. Hartman, M. Hassinen, C. Hayward, K. Heikkila, K. H. Herzig, Q. Helmer, H. L. Hillege, O. Holmen, S. C. Hunt, A. Isaacs, T. Ittermann, A. L. James, I. Johansson, T. Juliusdottir, I. P. Kalafati, L. Kinnunen, W. Koenig, I. K. Kooner, W. Kratzer, C. Lamina, K. Leander, N. R. Lee, P. Lichtner, L. Lind, J. Lindstrom, S. Lobbens, M. Lorentzon, F. Mach, P. K. Magnusson, A. Mahajan, W. L. McArdle, C. Menni, S. Merger, E. Mihailov, L. Milani, R. Mills, A. Moayyeri, K. L. Monda, S. P. Mooijaart, T. W. Muhleisen, A. Mulas, G. Muller, M. Muller-Nurasyid, R. Nagaraja, M. A. Nalls, N. Narisu, N. Glorioso, I. M. Nolte, M. Olden, N. W. Rayner, F. Renstrom, J. S. Ried, N. R. Robertson, L. M. Rose, S. Sanna, H. Scharnagl, S. Scholtens, B. Sennblad, T. Seufferlein, C. M. Sitlani, A. Vernon Smith, K. Stirrups, H. M. Stringham, J. Sundstrom, M. A. Swertz, A. J. Swift, A. C. Syvanen, B. O. Tayo, B. Thorand, G. Thorleifsson, A. Tomaschitz, C. Troffa, F. V. van Oort, N. Verweij, J. M. Vonk, L. L. Waite, R. Wennauer, T. Wilsgaard, M. K. Wojczynski, A. Wong, Q. Zhang, J. Hua Zhao, E. P. Brennan, M. Choi, P. Eriksson, L. Folkersen, A. Franco-Cereceda, A. G. Gharavi, A. K. Hedman, M. F. Hivert, J. Huang, S. Kanoni, F. Karpe, S. Keildson, K. Kiryluk, L. Liang, R. P. Lifton, B. Ma, A. J. McKnight, R. McPherson, A. Metspalu, J. L. Min, M. F. Moffatt, G. W. Montgomery, J. M. Murabito, G. Nicholson, D. R. Nyholt, C. Olsson, J. R. Perry, E. Reinmaa, R. M. Salem, N. Sandholm, E. E. Schadt, R. A. Scott, L. Stolk, E. E. Vallejo, H. J. Westra, K. T. Zondervan, A. D. Consortium, C. A. D. Consortium, C. K. Consortium, G. Consortium, G. Consortium, Glgc, Icbp, C. International Endogene, S. LifeLines Cohort, M. Investigators, T. C. Mu, P. Consortium, C. ReproGen, P. Amouyel, D. Arveiler, S. J. Bakker, J. Beilby, R. N. Bergman, J. Blangero, M. J. Brown, M. Burnier, H. Campbell, A. Chakravarti, P. S. Chines, S. Claudi-

Boehm, F. S. Collins, D. C. Crawford, J. Danesh, U. de Faire, E. J. de Geus, M. Dorr, R. Erbel, J. G. Eriksson, M. Farrall, E. Ferrannini, J. Ferrieres, N. G. Forouhi, T. Forrester, O. H. Franco, R. T. Gansevoort, C. Gieger, V. Gudnason, C. A. Haiman, T. B. Harris, A. T. Hattersley, M. Heliovaara, A. A. Hicks, A. D. Hingorani, W. Hoffmann, A. Hofman, G. Homuth, S. E. Humphries, E. Hypponen, T. Illig, M. R. Jarvelin, B. Johansen, P. Jousilahti, A. M. Jula, J. Kaprio, F. Kee, S. M. Keinanen-Kiukaanniemi, J. S. Kooner, C. Kooperberg, P. Kovacs, A. T. Kraja, M. Kumari, K. Kuulasmaa, J. Kuusisto, T. A. Lakka, C. Langenberg, L. Le Marchand, T. Lehtimaki, V. Lyssenko, S. Mannisto, A. Marette, T. C. Matise, C. A. McKenzie, B. McKnight, A. W. Musk, S. Mohlenkamp, A. D. Morris, M. Nelis, C. Ohlsson, A. J. Oldehinkel, K. K. Ong, L. J. Palmer, B. W. Penninx, A. Peters, P. P. Pramstaller, O. T. Raitakari, T. Rankinen, D. C. Rao, T. K. Rice, P. M. Ridker, M. D. Ritchie, I. Rudan, V. Salomaa, N. J. Samani, J. Saramies, M. A. Sarzynski, P. E. Schwarz, A. R. Shuldiner, J. A. Staessen, V. Steinthorsdottir, R. P. Stolk, K. Strauch, A. Tonjes, A. Tremblay, E. Tremoli, M. C. Vohl, U. Volker, P. Vollenweider, J. F. Wilson, J. C. Witteman, L. S. Adair, M. Bochud, B. O. Boehm, S. R. Bornstein, C. Bouchard, S. Cauchi, M. J. Caulfield, J. C. Chambers, D. I. Chasman, R. S. Cooper, G. Dedoussis, L. Ferrucci, P. Froguel, H. J. Grabe, A. Hamsten, J. Hui, K. Hveem, K. H. Jockel, M. Kivimaki, D. Kuh, M. Laakso, Y. Liu, W. Marz, P. B. Munroe, I. Njolstad, B. A. Oostra, C. N. Palmer, N. L. Pedersen, M. Perola, L. Perusse, U. Peters, C. Power, T. Quertermous, R. Rauramaa, F. Rivadeneira, T. E. Saaristo, D. Saleheen, J. Sinisalo, P. E. Slagboom, H. Snieder, T. D. Spector, U. Thorsteinsdottir, M. Stumvoll, J. Tuomilehto, A. G. Uitterlinden, M. Uusitupa, P. van der Harst, G. Veronesi, M. Walker, N. J. Wareham, H. Watkins, H. E. Wichmann, G. R. Abecasis, T. L. Assimes, S. I. Berndt, M. Boehnke, I. B. Borecki, P. Deloukas, L.

Franke, T. M. Frayling, L. C. Groop, D. J. Hunter, R. C. Kaplan, J. R. O'Connell, L. Qi, D. Schlessinger, D. P. Strachan, K. Stefansson, C. M. van Duijn, C. J. Willer, P. M. Visscher, J. Yang, J. N. Hirschhorn, M. C. Zillikens, M. I. McCarthy, E. K. Speliotes, K. E. North, C. S. Fox, I. Barroso, P. W. Franks, E. Ingelsson, I. M. Heid, R. J. Loos, L. A. Cupples, A. P. Morris, C. M. Lindgren, and K. L. Mohlke. 2015. New genetic loci link adipose and insulin biology to body fat distribution. *Nature* **518**: 187-196.

29. Heid, I. M., A. U. Jackson, J. C. Randall, T. W. Winkler, L. Qi, V. Steinthorsdottir, G. Thorleifsson, M. C. Zillikens, E. K. Speliotes, R. Magi, T. Workalemahu, C. C. White, N. Bouatia-Naji, T. B. Harris, S. I. Berndt, E. Ingelsson, C. J. Willer, M. N. Weedon, J. Luan, S. Vedantam, T. Esko, T. O. Kilpelainen, Z. Kutalik, S. Li, K. L. Monda, A. L. Dixon, C. C. Holmes, L. M. Kaplan, L. Liang, J. L. Min, M. F. Moffatt, C. Molony, G. Nicholson, E. E. Schadt, K. T. Zondervan, M. F. Feitosa, T. Ferreira, H. Lango Allen, R. J. Weyant, E. Wheeler, A. R. Wood, Magic, K. Estrada, M. E. Goddard, G. Lettre, M. Mangino, D. R. Nyholt, S. Purcell, A. V. Smith, P. M. Visscher, J. Yang, S. A. McCarroll, J. Nemesh, B. F. Voight, D. Absher, N. Amin, T. Aspelund, L. Coin, N. L. Glazer, C. Hayward, N. L. Heard-Costa, J. J. Hottenga, A. Johansson, T. Johnson, M. Kaakinen, K. Kapur, S. Ketkar, J. W. Knowles, P. Kraft, A. T. Kraja, C. Lamina, M. F. Leitzmann, B. McKnight, A. P. Morris, K. K. Ong, J. R. Perry, M. J. Peters, O. Polasek, I. Prokopenko, N. W. Rayner, S. Ripatti, F. Rivadeneira, N. R. Robertson, S. Sanna, U. Sovio, I. Surakka, A. Teumer, S. van Wingerden, V. Vitart, J. H. Zhao, C. Cavalcanti-Proenca, P. S. Chines, E. Fisher, J. R. Kulzer, C. Lecoeur, N. Narisu, C. Sandholt, L. J. Scott, K. Silander, K. Stark, M. L. Tammesoo, T. M. Teslovich, N. J. Timpson, R. M. Watanabe, R. Welch, D. I. Chasman, M. N. Cooper, J. O. Jansson, J. Kettunen, R. W. Lawrence, N. Pellikka, M. Perola, L.

Vandenput, H. Alavere, P. Almgren, L. D. Atwood, A. J. Bennett, R. Biffar, L. L. Bonnycastle, S. R. Bornstein, T. A. Buchanan, H. Campbell, I. N. Day, M. Dei, M. Dorr, P. Elliott, M. R. Erdos, J. G. Eriksson, N. B. Freimer, M. Fu, S. Gaget, E. J. Geus, A. P. Gjesing, H. Grallert, J. Grassler, C. J. Groves, C. Guiducci, A. L. Hartikainen, N. Hassanali, A. S. Havulinna, K. H. Herzig, A. A. Hicks, J. Hui, W. Igl, P. Jousilahti, A. Jula, E. Kajantie, L. Kinnunen, I. Kolcic, S. Koskinen, P. Kovacs, H. K. Kroemer, V. Krzelj, J. Kuusisto, K. Kvaloy, J. Laitinen, O. Lantieri, G. M. Lathrop, M. L. Lokki, R. N. Luben, B. Ludwig, W. L. McArdle, A. McCarthy, M. A. Morken, M. Nelis, M. J. Neville, G. Pare, A. N. Parker, J. F. Peden, I. Pichler, K. H. Pietilainen, C. G. Platou, A. Pouta, M. Ridderstrale, N. J. Samani, J. Saramies, J. Sinisalo, J. H. Smit, R. J. Strawbridge, H. M. Stringham, A. J. Swift, M. Teder-Laving, B. Thomson, G. Usala, J. B. van Meurs, G. J. van Ommen, V. Vatin, C. B. Volpato, H. Wallaschofski, G. B. Walters, E. Widen, S. H. Wild, G. Willemsen, D. R. Witte, L. Zgaga, P. Zitting, J. P. Beilby, A. L. James, M. Kahonen, T. Lehtimaki, M. S. Nieminen, C. Ohlsson, L. J. Palmer, O. Raitakari, P. M. Ridker, M. Stumvoll, A. Tonjes, J. Viikari, B. Balkau, Y. Ben-Shlomo, R. N. Bergman, H. Boeing, G. D. Smith, S. Ebrahim, P. Froguel, T. Hansen, C. Hengstenberg, K. Hveem, B. Isomaa, T. Jorgensen, F. Karpe, K. T. Khaw, M. Laakso, D. A. Lawlor, M. Marre, T. Meitinger, A. Metspalu, K. Midthjell, O. Pedersen, V. Salomaa, P. E. Schwarz, T. Tuomi, J. Tuomilehto, T. T. Valle, N. J. Wareham, A. M. Arnold, J. S. Beckmann, S. Bergmann, E. Boerwinkle, D. I. Boomsma, M. J. Caulfield, F. S. Collins, G. Eiriksdottir, V. Gudnason, U. Gyllensten, A. Hamsten, A. T. Hattersley, A. Hofman, F. B. Hu, T. Illig, C. Iribarren, M. R. Jarvelin, W. H. Kao, J. Kaprio, L. J. Launer, P. B. Munroe, B. Oostra, B. W. Penninx, P. P. Pramstaller, B. M. Psaty, T. Quertermous, A. Rissanen, I. Rudan, A. R. Shuldiner, N. Soranzo, T. D. Spector,

A. C. Syvanen, M. Uda, A. Uitterlinden, H. Volzke, P. Vollenweider, J. F. Wilson, J. C. Witteman, A. F. Wright, G. R. Abecasis, M. Boehnke, I. B. Borecki, P. Deloukas, T. M. Frayling, L. C. Groop, T. Haritunians, D. J. Hunter, R. C. Kaplan, K. E. North, J. R. O'Connell, L. Peltonen, D. Schlessinger, D. P. Strachan, J. N. Hirschhorn, T. L. Assimes, H. E. Wichmann, U. Thorsteinsdottir, C. M. van Duijn, K. Stefansson, L. A. Cupples, R. J. Loos, I. Barroso, M. I. McCarthy, C. S. Fox, K. L. Mohlke, and C. M. Lindgren. 2010. Meta-analysis identifies 13 new loci associated with waist-hip ratio and reveals sexual dimorphism in the genetic basis of fat distribution. *Nat Genet* **42**: 949-960.

30. Mejhert, N., F. Wilfling, D. Esteve, J. Galitzky, V. Pellegrinelli, C. I. Kolditz, N. Viguerie, J. Tordjman, E. Naslund, P. Trayhurn, D. Lacasa, I. Dahlman, V. Stich, P. Lang, D. Langin, A. Bouloumie, K. Clement, and M. Ryden. 2013. Semaphorin 3C is a novel adipokine linked to extracellular matrix composition. *Diabetologia* **56**: 1792-1801.

31. Shimizu, I., Y. Yoshida, J. Moriya, A. Nojima, A. Uemura, Y. Kobayashi, and T. Minamino. 2013. Semaphorin3E-induced inflammation contributes to insulin resistance in dietary obesity. *Cell Metab* **18**: 491-504.

32. Walton, R. G., X. Zhu, L. Tian, E. B. Heywood, J. Liu, H. S. Hill, J. Liu, D. Bruemmer, Q. Yang, Y. Fu, and W. T. Garvey. 2016. AP2-NR4A3 transgenic mice display reduced serum epinephrine because of increased catecholamine catabolism in adipose tissue. *Am J Physiol Endocrinol Metab* **311**: E69-81.

33. Wilson, A. M., Z. Shao, V. Grenier, G. Mawambo, J. F. Daudelin, A. Dejda, F. Pilon, N. Popovic, S. Boulet, C. Parinot, M. Oubaha, N. Labrecque, V. de Guire, M. Laplante, G. Lettre, F. Sennlaub, J. S. Joyal, M. Meunier, and P. Sapieha. 2018. Neuropilin-1

expression in adipose tissue macrophages protects against obesity and metabolic syndrome. *Sci Immunol* **3**.

34. Loffler, D., S. Behrendt, J. W. Creemers, J. Klammt, G. Aust, J. Stanik, W. Kiess, P. Kovacs, and A. Korner. 2017. Functional and clinical relevance of novel and known PCSK1 variants for childhood obesity and glucose metabolism. *Mol Metab* **6**: 295-305.

35. Heinonen, S., J. Buzkova, M. Muniandy, R. Kaksonen, M. Ollikainen, K. Ismail, A. Hakkarainen, J. Lundbom, N. Lundbom, K. Vuolteenaho, E. Moilanen, J. Kaprio, A. Rissanen, A. Suomalainen, and K. H. Pietilainen. 2015. Impaired Mitochondrial Biogenesis in Adipose Tissue in Acquired Obesity. *Diabetes* **64**: 3135-3145.

36. Mirakaj, V., and P. Rosenberger. 2017. Immunomodulatory Functions of Neuronal Guidance Proteins. *Trends Immunol* **38**: 444-456.

37. Alvarez-Aznar, A., L. Muhl, and K. Gaengel. 2017. VEGF Receptor Tyrosine Kinases: Key Regulators of Vascular Function. *Curr Top Dev Biol* **123**: 433-482.

38. Minchin, J. E., I. Dahlman, C. J. Harvey, N. Mejhert, M. K. Singh, J. A. Epstein, P. Arner, J. Torres-Vazquez, and J. F. Rawls. 2015. Plexin D1 determines body fat distribution by regulating the type V collagen microenvironment in visceral adipose tissue. *Proc Natl Acad Sci U S A* **112**: 4363-4368.

39. Minchin, J. E. N., and J. F. Rawls. 2017. Elucidating the role of plexin D1 in body fat distribution and susceptibility to metabolic disease using a zebrafish model system. *Adipocyte*: 1-7.

40. Anderson, J. L., T. S. Mulligan, M. C. Shen, H. Wang, C. M. Scahill, F. J. Tan, S. J. Du, E. M. Busch-Nentwich, and S. A. Farber. 2017. mRNA processing in mutant zebrafish lines generated by chemical and CRISPR-mediated mutagenesis produces

unexpected transcripts that escape nonsense-mediated decay. *PLoS Genet* **13**: e1007105.

41. Colman, R. J., J. J. Ramsey, E. B. Roecker, T. Havighurst, J. C. Hudson, and J. W. Kemnitz. 1999. Body fat distribution with long-term dietary restriction in adult male rhesus macaques. *J Gerontol A Biol Sci Med Sci* **54**: B283-290.

42. Goss, A. M., L. L. Goree, A. C. Ellis, P. C. Chandler-Laney, K. Casazza, M. E. Lockhart, and B. A. Gower. 2013. Effects of diet macronutrient composition on body composition and fat distribution during weight maintenance and weight loss. *Obesity (Silver Spring)* **21**: 1139-1142.

43. Varady, K. A., C. A. Allister, D. J. Roohk, and M. K. Hellerstein. 2010. Improvements in body fat distribution and circulating adiponectin by alternate-day fasting versus calorie restriction. *J Nutr Biochem* **21**: 188-195.

Tables

Table 1. Zebrafish mutants assessed for adiposity changes in this study

Gene	Gene symbol	Allele	Allele consequence	# of fish screened	% misclassified ('phenotypic')
neuropilin 2b	*nrp2b*	sa18942	Essential splice site	34	35.3%
nuclear receptor subfamily group a member 3	*nr4a3*	sa2842	Nonsense	34	14.7%
proprotein convertase subtilisin/kexin type 1	*pcsk1*	sa1558	Essential splice site	33	9%
semaphorin 3aa	*sema3aa*	sa10241	Nonsense	35	14%
semaphorin 3fb	*sema3fb*	sa14466	Nonsense	47	14.8%
semaphorin 3gb	*sema3gb*	sa21283	Nonsense	21	14.2%
sarcospan	*sspn*	sa2992	Nonsense	36	16.7%
transmembrane protein 160	*tmem160*	sa1347	Nonsense	29	13.7%

growth hormone	*gh*	wp22e1	Premature stop codon	130	36%

Table 2. Morphological traits used to construct adiposity profiles.

Trait	**Trait acronym**	**Trait category**
Standard length (µm)	SL	Body size
Height at anterior of anal fin (µm)	HAA	Body size
Body area (µm^2)	BA	Body size
Pancreatic VAT (µm^2)	PVAT	AT area
Abdominal VAT (µm^2)	AVAT	AT area
Renal VAT (µm^2)	RVAT	AT area
Cardiac VAT (µm^2)	CVAT	AT grouping
Anterior CVAT (µm^2)	aCVAT	AT area
Posterior CVAT (µm^2)	pCVAT	AT area
Visceral AT (µm^2)	VAT	AT area
Abdominal SAT (µm^2)	ASAT	AT area
Lateral SAT (µm^2)	LSAT	AT area
Dorsal SAT (µm^2)	DSAT	AT grouping
Anterior DSAT (µm^2)	aDSAT	AT area
Posterior DSAT (µm^2)	pDSAT	AT area
Ventral SAT (µm^2)	VSAT	AT area

Truncal SAT (μm^2)	TSAT	AT grouping
Dorsal fin ray SAT (μm^2)	DFRSAT	AT area
Anal fin ray cluster SAT (μm^2)	AFCSAT	AT area
Anal fin ray SAT (μm^2)	AFRSAT	AT area
Caudal fin ray SAT (μm^2)	CFRSAT	AT area
Pectoral fin SAT (μm^2)	PECSAT	AT grouping
Loose PECSAT (μm^2)	lPECSAT	AT area
Anterior PECSAT (μm^2)	aPECSAT	AT area
Posterior PECSAT (μm^2)	pPECSAT	AT area
Appendicular SAT (μm^2)	APPSAT	AT grouping
Central IM (μm^2)	cIM	AT area
Dorsal IM (μm^2)	dIM	AT area
Ventral IM (μm^2)	vIM	AT area
Intermuscular (μm^2)	IM	AT grouping
Dorsal POS (μm^2)	dPOS	AT area
Central POS (μm^2)	cPOS	AT area
Ventral POS (μm^2)	vPOS	AT area
Paraosseal (μm^2)	POS	AT grouping
Oesophageal (μm^2)	OES	AT area
Non-visceral AT (μm^2)	NVAT	AT grouping
Dorsal OPC (μm^2)	dOPC	AT area
Ventral OPC (μm^2)	vOPC	AT area

Opercular (μm^2)	OPC	AT grouping
Ocular (μm^2)	OCU	AT area
Branchihyal (μm^2)	BHD	AT area
Ceratohyal (μm^2)	CHD	AT area
Urihyal (μm^2)	UHD	AT area
Hyal (μm^2)	HYD	AT grouping
Cranial SAT (μm^2)	CSAT	AT grouping
Total AT (μm^2)	TOTAL	AT grouping
Subcutaneous AT (μm^2)	SAT	AT grouping
Internal AT (μm^2)	IAT	AT grouping
	VAT:IAT	AT ratio
	NVAT:IAT	AT ratio
	IAT:TOTAL	AT ratio
	SAT:TOTAL	AT ratio
	CSAT:SAT	AT ratio
	APPSAT:SAT	AT ratio
	TSAT:SAT	AT ratio
	VAT:SAT	AT ratio
	NVAT:SAT	AT ratio
	CSAT:IAT	AT ratio
	TSAT:IAT	AT ratio
	APPSAT:IAT	AT ratio
	VAT:TSAT	AT ratio

	VAT:CSAT	AT ratio
	VAT:APPSAT	AT ratio
	NVAT:TSAT	AT ratio
	NVAT:CSAT	AT ratio
	NVAT:APPSAT	AT ratio
	NVAT:VAT	AT ratio
	TSAT:CSAT	AT ratio
	APPSAT:CSAT	AT ratio
	APPSAT:TSAT	AT ratio

Figures

Figure 1

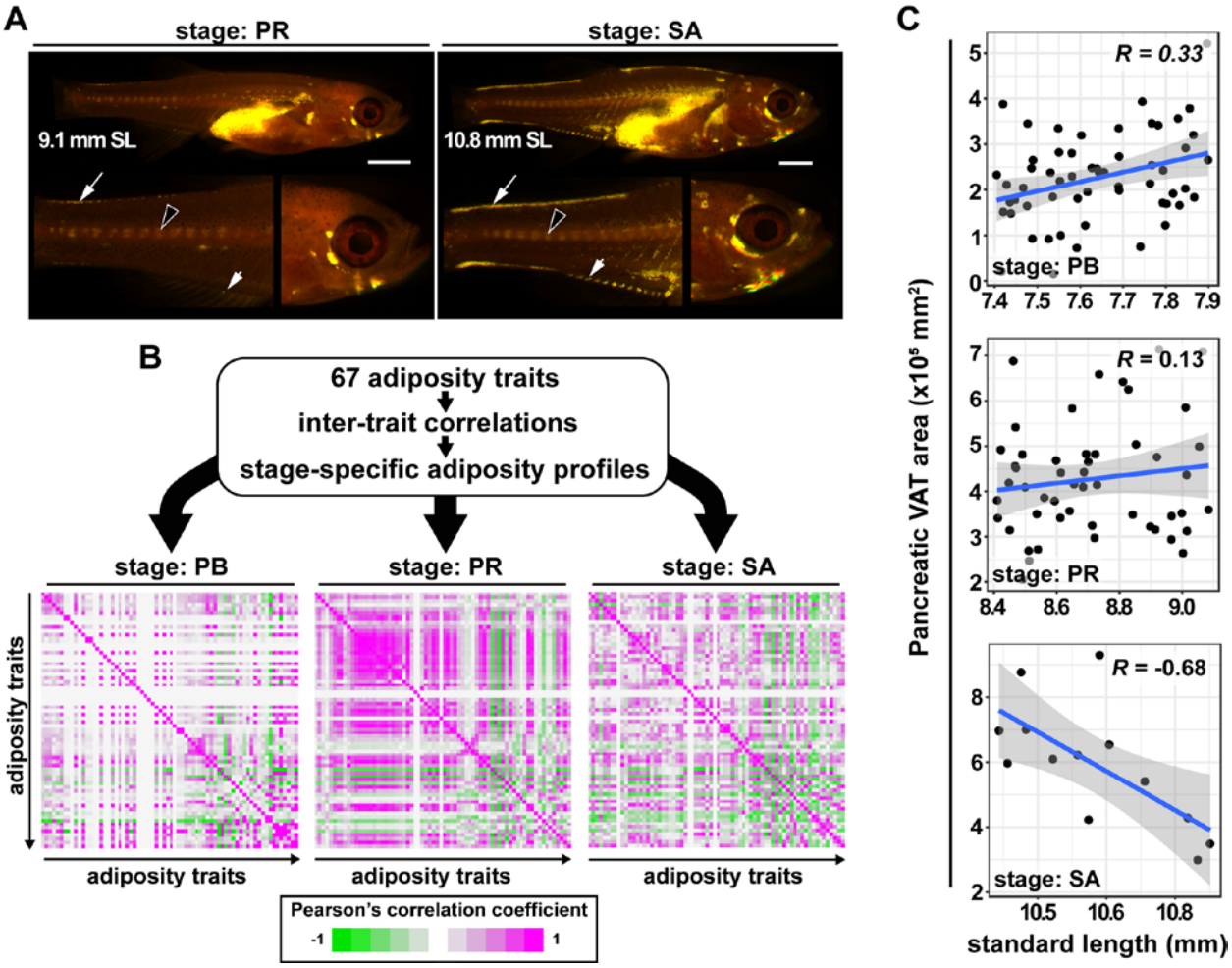

Figure 1. Generation of stage-specific adiposity profiles in zebrafish. A. Fluorescence stereomicroscope images of Nile Red stained zebrafish at two distinct postembryonic stages (PR and SA). Note the increasingly complex and diversifying distribution patterns of AT in SA fish relative to PR. White arrows correspond to pDSAT (posterior dorsal SAT), black arrowheads correspond to cPOS (central paraosseal), and white arrowheads correspond to AFRSAT (anal fin ray SAT). **B.** To determine wild-type adiposity dynamics, 67 adiposity traits were measured in 456 wild-type zebrafish. PB

denotes the pectoral fin bud stage from Parichy et al (2009). Each stage consisted of >10 fish. For each stage, inter-trait correlations were determined and used to create an adiposity profile that encapsulates relationship dynamics of individual ATs. **C.** Example inter-trait correlations are given for PVAT (pancreatic VAT) and demonstrate the changing relationship between PVAT and standard length (SL) across distinct stages.

Figure 2

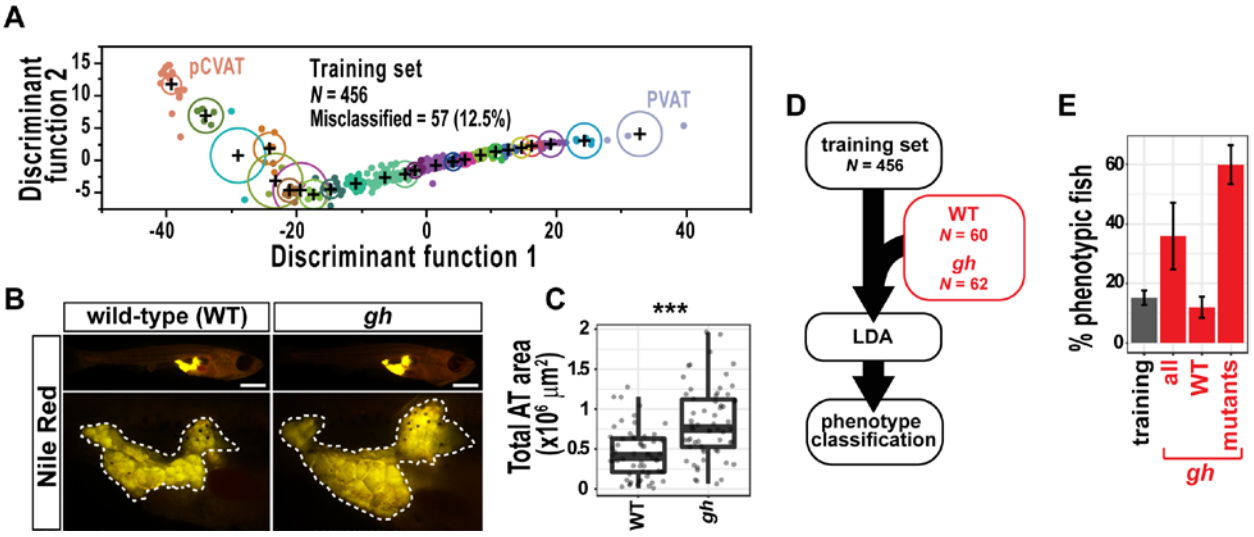

Figure 2. Linear discriminant analysis can be used to identify and classify phenotypic fish based on adiposity profiles. A. Linear discriminant analysis (LDA) was used as a training set to classify 456 wild-type fish according to stage-specific adiposity profiles. From this training set, LDA was able to accurately classify fish based on adiposity profiles in 87.5% of instances. **B.** Zebrafish homozygous for the *growth hormone* (*gh*) wp22e1 mutation have increased total AT (dotted outlines delineate AT). **C.** Quantification of total AT area in wild-type sibling and *gh* mutants. Student's t-test, *** = P<0.0001. **D.** Schematic detailing how the linear discriminant analysis was used to analyse *gh* mutant and wild-type (WT) sibling fish relative to the training set. **E.** Of the 122 *gh* and WT sibling fish, linear discriminant analysis detected 36% as phenotypic (all). The WT sibling fish were not classified as phenotypic relative to baseline classification from the training set (WT). The *gh* homozygous mutant fish were classified as phenotypic in 60% instances.

Figure 3

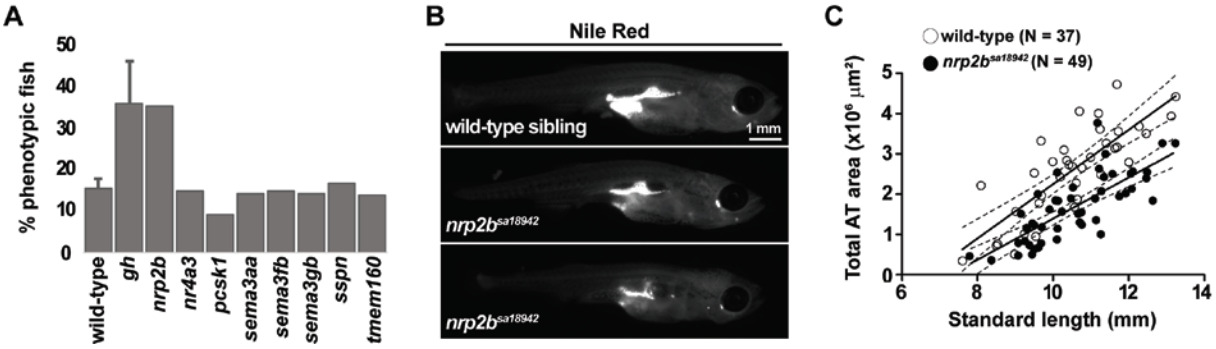

Figure 3. Linear discriminant analysis can be used as a screening tool to identify mutants with adiposity phenotypes in zebrafish. A. LDA misclassification rates (% phenotypic fish) for the eight ZMP mutants, *gh* mutants (positive control) and the wild-type training set. Error bars denote the standard error from the mean across multiple clutches. Bars without error bars are from single clutches. Details of the alleles for each mutant line can be found in **Table 1**. **B.** Fluorescence stereomicroscope images of Nile Red stained wild-type sibling and two *nrp2b*^{sa18942} homozygous mutant zebrafish. Note the reduced adiposity levels in *nrp2b*^{sa18942} mutants. **C.** Two additional independent clutches of wild-type siblings and *nrp2b*^{sa18942} mutants were assessed to validate the *nrp2b* phenotype. Linear regression (straight lines with 95% confidence intervals noted) was used to evaluate adiposity relative to SL, and ANCOVA was used to test for differences between the groups. $F_{1,83} = 52.4$, $P < 0.0001$.

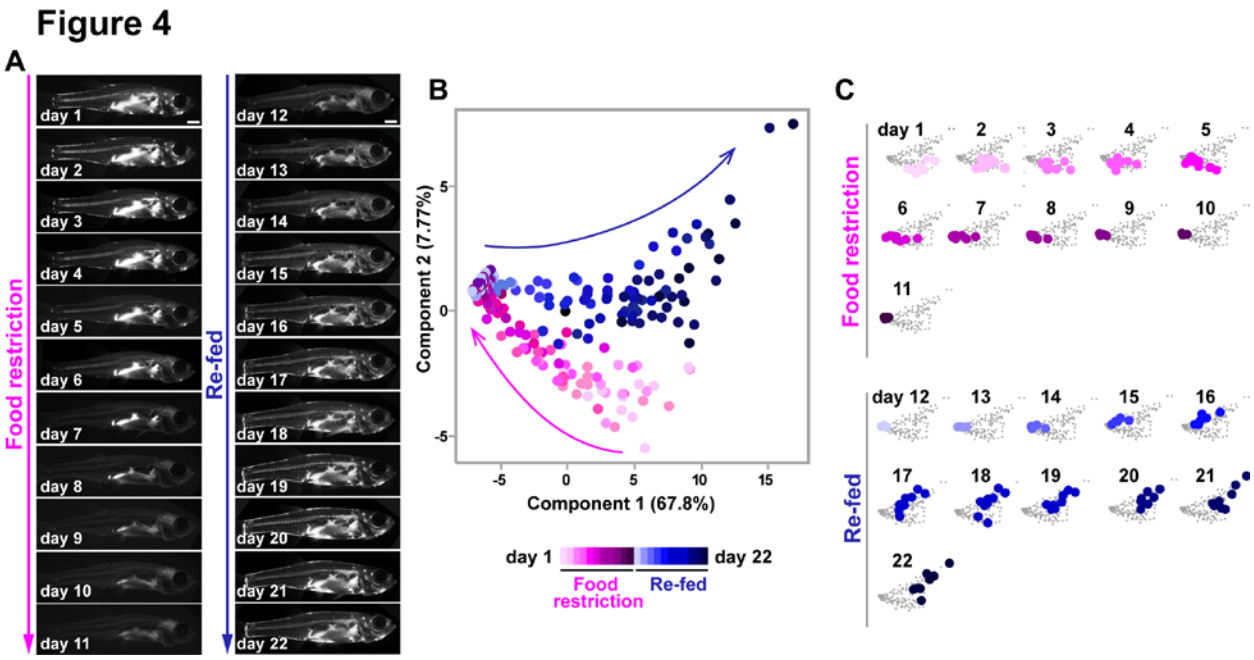

Figure 4. Food restriction and subsequent re-feeding leads to changes in adipose distribution. A. Fluorescence stereomicroscope images of Nile Red stained zebrafish reveal the mobilization and reduction of lipid within adipose tissue during 11 days of food restriction (magenta, days 1-11), and the re-deposition and increase in lipid within adipose during 11 days of re-feeding (blue, days 12-22). **B.** Principal components analysis of adiposity traits during food restriction and re-feeding reveals that food restriction leads to altered adipose distribution. Note that fed fish (light magenta, day 1) do not co-localize with re-fed animals (dark blue, day 22). **C.** Principal components analysis of food restriction and re-feeding reveals the daily changes in adipose distribution.

Figure 5

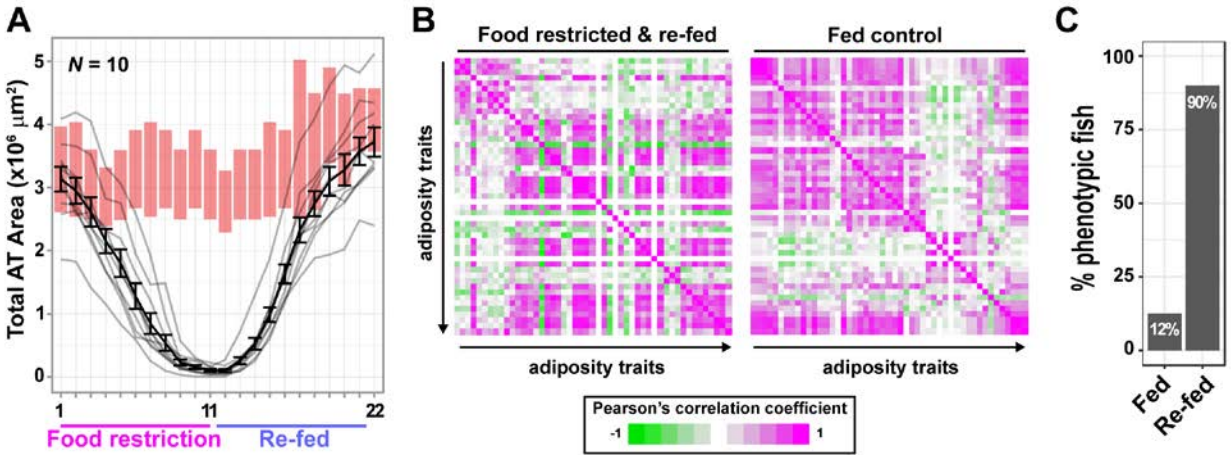

Figure 5. Linear discriminant analysis can be used to classify food restriction-induced changes in adiposity. A. Chart showing the reduction and subsequent re-gain of total AT area during food restriction (days 1-11) and re-feeding (days 12-22). Black line connects the mean total AT area at each day. Black error bars at each day denote the standard deviation in total AT area. Grey lines indicate the total AT area of individual fish. Red bars indicate the standard deviation of total AT area of size-matched fed animals. Note that at day 22, re-fed animals have re-gained total AT to an equivalent level as size-matched continuously fed animals. **B.** Adiposity profiles showing inter-trait correlations at stage DFRSAT in food restricted/re-fed animals and size-matched continuously fed animals. **C.** Linear discriminant analysis classifies food restricted/re-fed animals as phenotypic in 90% of instances.

Figure 6

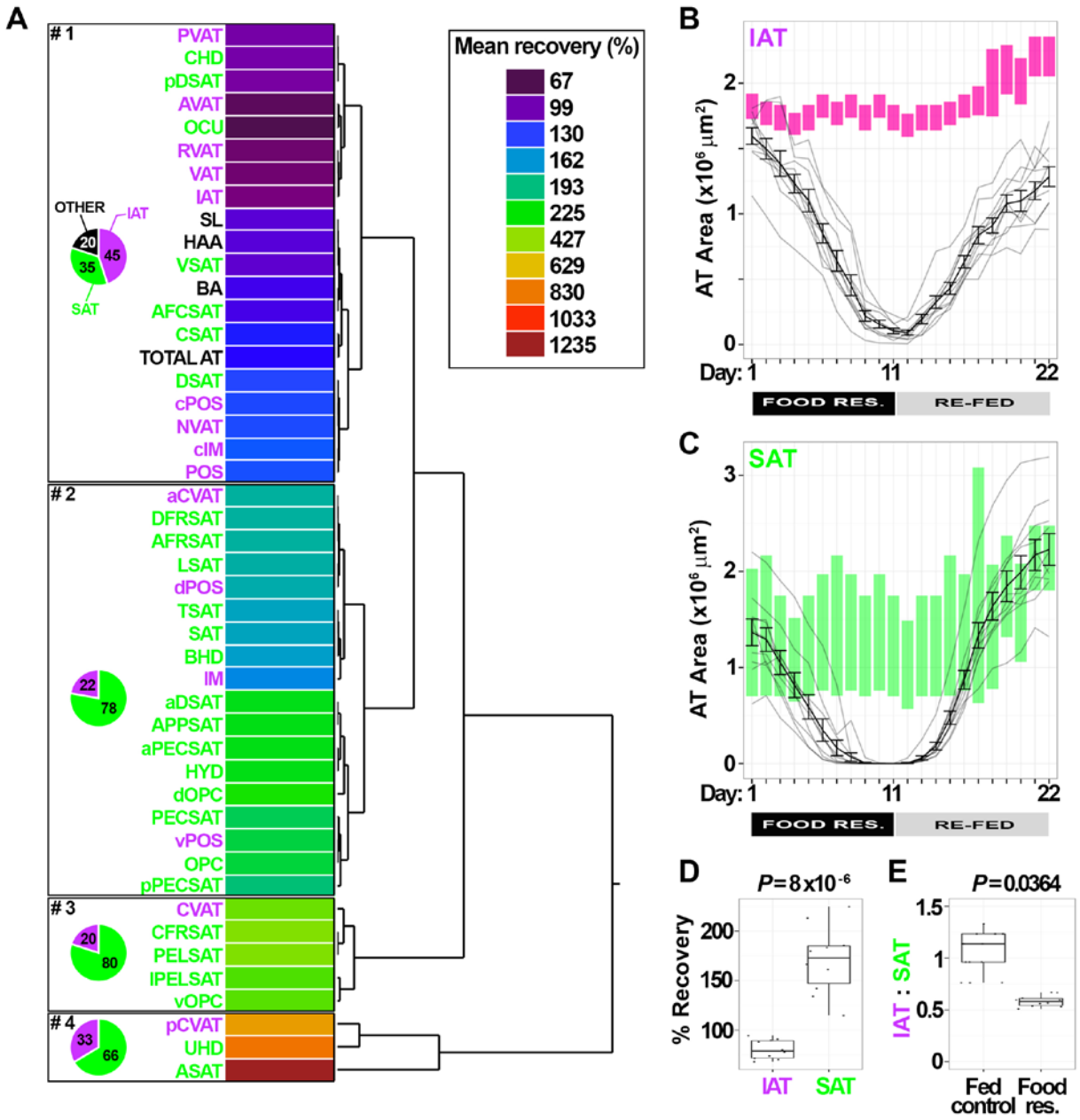

Figure 6. Internal adipose tissues have a decreased capacity to replenish lipid stores following food restriction. A. Hierarchical clustering of individual ATs based on % replenishment of lipid (day 22 lipid as a % of day 1 lipid). Four clusters were identified (#1-4) and ranked according to replenishment rates. Colour-code indicates % lipid replenishment (purple/blue = low, green/red = high). Internal ATs (IAT) are coloured

magenta. SAT are coloured green, and non-AT measures (e.g., SL) are coloured black. Pie charts depict the proportion of AT types in each cluster. Note, that clusters that replenish lipid to a high degree (i.e., clusters #3 & 4) and increasingly composed of SATs. **B,C.** AT-lipid mobilization and replenishment dynamics over the course of food-restriction (days 1-11) and re-feeding (days 12-22). The black line links mean AT area values at each timepoint. The black error bars denote standard deviation around the mean at each timepoint. The grey lines denote each individual fish (*N* = 10). The red (IAT; B) or green (SAT; C) bars denote the standard deviation around the mean of size & stage-matched 'continuously-fed' wild-type fish. These bars represent the expected IAT and SAT quantities in 'normal' fish. Note, that IAT after food restriction and re-feeding does not recover to expected wild-type levels. **D.** The % recovery of IAT and SAT reveals significant differences between the distinct AT divisions. **E.** The IAT:SAT ratio is significantly reduced in food restricted and re-fed animals (day 22) when compared to size and stage-matched 'continuously-fed' fish.